2013

Massive Quiescent Disk Galaxies in the CANDELS Survey

Aurora Y. Kesseli
Colby College

Massive Quiescent Disk Galaxies in the CANDELS Survey

Aurora Y. Kesseli

Department of Physics and Astronomy, Colby College

4000 Mayflower Hill, Waterville, ME 04901

A Thesis Presented to the Faculty of Colby College

May 2013

Advisor:

Elizabeth McGrath

ABSTRACT

We used data from the GOODS-S field of the CANDELS survey in order to confirm previous studies that found that large fractions of high-redshift galaxies (z $\sim$ 2) are disk-dominated (McGrath et al. 2008; van der Wel et al. 2011). In the GOODS-S field we selected out all the massive quiescent disk galaxies by imposing a mass limit of $M > 10^{10} M_{\odot}$ and a redshift range of $0.5 \leq z \leq 2.5$, and then choosing the quiescent red galaxies from a color-color plot. Once we had our sample, we did a qualitative visual classification of each galaxy and then a quantitative classification using the galaxy fitting program GALFIT. Our results from the fitting showed that 23 of the original 140 galaxies were classified as disk-dominated by GALFIT, and on further study we saw that most of these were at high-redshift. At a redshift of z $\sim$ 2 a significant fraction of galaxies showed strong disk components and 30% of them were disk-dominated. We also saw that the massive disk galaxies and the massive elliptical galaxies live in two different environments. The disk galaxies seem to live in less densely populated areas, which leads us to believe that there are two mechanisms for the creation of massive quiescent galaxies, one which creates the disks and one which creates the massive elliptical galaxies. For the disks, our observations imply a period of rapid star-formation in the early universe, but only after the majority of the gas had settled into a disk. The lower density environment and the disk nature of these galaxies leads us to favor cold streams over the major merger model of galaxy formation. For the ellipticals, which live in higher density environments, it is possible that major mergers of already aged stellar populations (e.g., dry mergers) could be the primary assembly mechanism.

1. Introduction

The evolution of galaxies from smaller, blue, star-forming galaxies to larger, red, non-star-forming (quiescent) galaxies is a process that is still difficult to concretely explain. In our present day universe there is a bimodality in color and morphology, and all of the massive galaxies are also all red in color and are observed to be spheroidal galaxies (see Figure 1). Massive galaxies cannot just form through monolithic gravitational collapse at early times since the over-densities present shortly after the big bang were not large enough to fuel such large galaxy formation. Furthermore, the most massive galaxies today all appear to be quiescent ellipticals, so the natural explanation of the reddening process involves the merging of these spiral galaxies formed early in the history of the universe. When the two galaxies collide there is a burst of star formation because all the gas and dust from the two merging galaxies is mixed together and collapses into stars. This is followed by a period characterized by no new star formation since all the gas has been used up. Blue stars are very bright but also have short lifetimes and so as the galaxy ages only the long-lasting red stars are left and so the galaxy in turn becomes more red. Through simulations of mergers we expect the end product of colliding galaxies to be a spheroidal galaxy (Toomre 1977; Barnes 1988; Barnes & Hernquist 1992; Hernquist 1992). However, recent studies (McGrath et al. 2008; van der Wel et al. 2011) find that at z $\sim$ 2 around 50% of galaxies that are quiescent are also disk-like. This would imply that there must be some mechanism that creates massive quiescent galaxies other than mergers. Previous studies suffer from small number statistics because it was difficult to get high-resolution images of highly redshifted galaxies before wide-field infrared surveys such as CANDELS. CANDELS (see §2) provides the first large sample of these highly redshifted galaxies so we were able to expand the scope of the previous surveys in order to address the question of massive galaxy formation in a statistically meaningful way.

In order to gain insight on this process we selected massive galaxies because even though massive galaxies are rare, they are so large that more than half of the luminous matter in the universe is contained in these massive elliptical galaxies in the present day universe (Fukugita et al. 1998; Bell et al. 2003). Then, to test the above theories we need to trace the morphological history of galaxies over time.

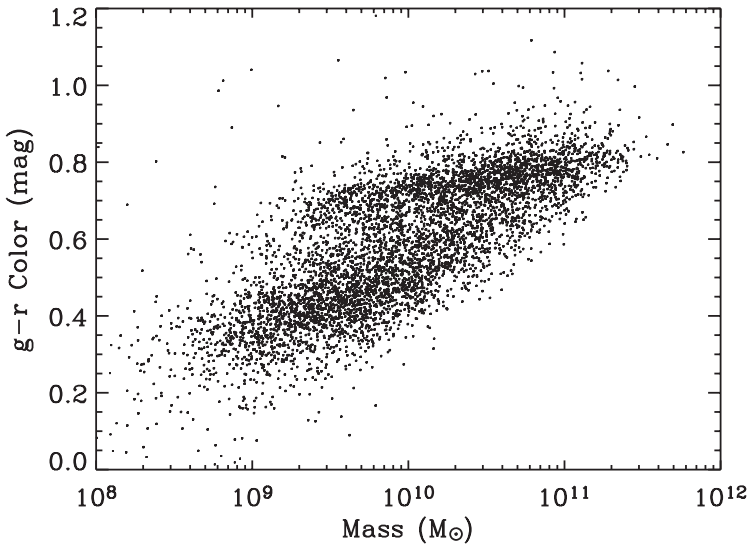

Fig. 1.— Plot of the color of observed galaxies versus the mass. The plot shows that all of the most massive galaxies are also all red in color. These red massive galaxies have all been observed to be spheroidal galaxies, demonstrating that locally all the massive galaxies are red spheroidal galaxies. Taken from Baldry et al. (2004)

2. CANDELS Data

The observing program CANDELS, or Cosmic Assembly Near-Infrared Deep Extragalactic Legacy Survey (Grogin et al. 2011; Koekemoer et al. 2011) provides an excellent set of data in order to try to answer these questions of galaxy evolution because it can detect highly redshifted galaxies at a high-resolution. Once completed in mid-2013, the survey will

include images of over 250,000 distant galaxies from redshifts going all the way back to z $\sim$ 8 in five different fields at two different depths (Grogin et al. 2011). The five fields include the GOODS-N or Great Observatories Origins Deep Survey (Giavalisco et al. 2004), GOODS-S (Giavalisco et al. 2004), EGS or Extended Groth Strip (Davis et al. 2007), UDS or Ultra Deep Survey (Lawrence et al. 2007), and COSMOS (Scoville et al. 2007). The two depths are a wide shallow field and a deep but smaller area survey only located in the GOODS-N and GOODS-S regions. The CANDELS data was collected using three different cameras on the Hubble Space Telescope (HST) in multiple wavelength from the mid-ultraviolet to the near-infrared (Grogin et al. 2011). Because HST's Wide Field Camera 3 (WFC3) observes in the near-infrared it can see the highly redshifted galaxies and because the data is taken with such a powerful space telescope like Hubble, the GOODS fields possess the deepest and highest resolution data available right now.

We utilized CANDELS's WFC3 data from the GOODS-S field (Wide and Deep), located at 53.122751, -27.805089 as well as the WFC3's Early Release Science (ERS2) data (Windhorst et al. 2011) which is included in the GOODS-S field. The deep region is made up of about 3 x 5 Wide Field Camera 3 (WFC3) tiles in the infrared, whereas the Wide field is made up of about 2 x 4 tiles and the ERS about 2 x 5 (Grogin et al. 2011). Figure 2 shows the positions of the various tiles of the GOODS-S field. Each tile is a compilation of multiple pointings of the camera, and in the GOODS-S field the total exposure time per tile is approximately 5250 seconds (Koekemoer et al. 2011). Because the pixels are so large in the detector Koekemoer et al. (2011) use a four point small scale dither pattern in order to extract more detail from the observations. The dithered data are then combined with MultiDrizzle (Koekemoer et al. 2002) and then each tile is combined into a mosaic taking into account geometric distortion from the spherical deprojection. In order to learn more details about the mosaic compilation refer to Koekemoer et al. (2011).

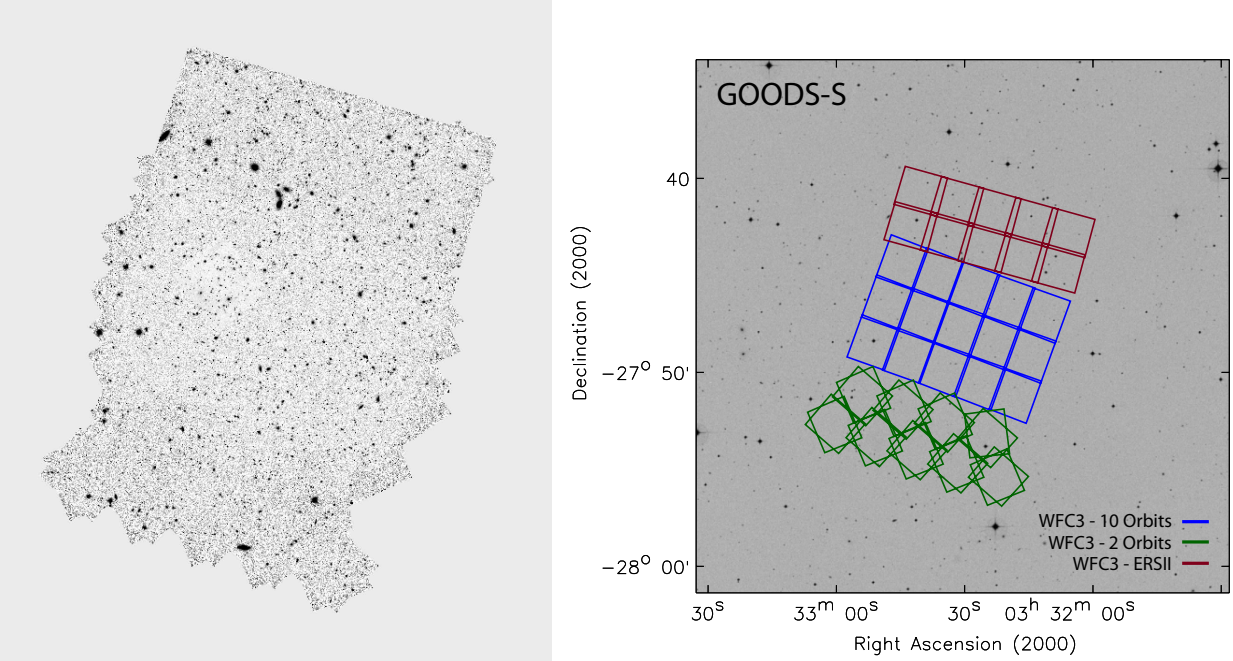

Fig. 2.— Left: Mosaic of the CANDELS GOODS-S field. Right: simplified map of CANDELS GOODS-S field, which was observed with the WFC3/IR camera on the Hubble Space Telescope. Reprinted from Grogin et al. (2011).

3. Galaxy Selection

We selected out the galaxies of interest from the entire sample according to redshift, mass and quiescent parameters set by Williams et al. (2009). van der Wel et al. (2011) state that morphology measurements are accurate up to 10% precision for galaxies with an H-band value of ~ 24.5 magnitudes. In order to stay within this precision limit we needed to set a consistent limit for both the mass and the redshift. We chose the mass constraint to be $M > 10^{10} M_{\odot}$, ensuring we selected only the most massive galaxies at an given epoch. With the mass limit set, we set our upper redshift limit at $z > 2.5$, since anything with $z > 2.5$ and $M > 10^{10} M_{\odot}$ would fall outside of the H-band magnitude limit and would not have accurate morphological measurements (Chang et al. 2013). The entire redshift range

we sampled was $0.5 \leq z \leq 2.5$ since below z = 0.5 the volume sampled by the CANDELS survey is insufficient to provide proper number statistics. This range allows us to compare a magnitude limited sample that is complete to $M > 10^{10} M_{\odot}$ at all redshifts.

To select out the quiescent galaxies we created a rest-frame U - V versus rest frame V - J diagram. In this type of color-color diagram Labbé et al. (2005) and Wuyts et al. (2007) showed that star-forming galaxies and quiescent galaxies occupy two distinct different areas. The star-forming galaxies form a diagonal line from the lower left to the upper right corner, while the quiescent galaxies form a clump above the diagonal track (see Figure 3). Williams et al. (2009) explains that this method is able to discern the red quiescent galaxies from the non-quiescent dust reddened galaxy very accurately because the quiescent galaxies that are not reddened by dust appear to be bluer in V - J since the spectral energy distributions for these galaxies peak in the visible. On the other hand, dust reddened galaxies peak in the infrared since when photons hit dust they are scattered and reemitted in the infrared and therefore the V-J for these galaxies appear to be more red. Williams et al. (2009) found the cutoff by using empirical criteria and then fine tuning this diagonal line to fall between the two different galaxy populations. They found three relations for different redshift bins ($0 < z < 0.5, 0.5 < z < 1.0, 1.0 < z < 2.0$) since as the redshift increases the rest frame colors are bluer. We chose to use the relation for the redshift bin $0.5 < z < 1.0$ since our redshift values started at 0.5 and this cutoff is more conservative, meaning it might miss a few galaxies but it should not include any of the star-forming galaxies at any redshift. If we had used the cutoff for the higher redshift value we would get all the quiescent galaxies but we would also pick up some dust reddened star-forming galaxies. The cutoffs that we used are as follows:

$$(U - V) \quad > \quad 0.88 \times (V - J) + 0.59 \tag{1}$$

$$\begin{aligned} U - V &> 1.3 \\ V - J &< 1.6 \end{aligned}$$

The second two parameters are just added so that no stray dust reddened galaxies end up in the sample. The CANDELS data provides a sersic index estimate through a one component galfit process, which will be explained in more detail in §4.1 (van der Wel et al. 2012). The sersic index describes the intensity of a galaxy profile with a number ranging from 0 to 20. Galaxies with low sersic indices are less centrally concentrated, so disk galaxies usually fall around a sersic index of 1. Spheroids are much more intense in the center and then the intensity falls off and these galaxies usually have a sersic index greater than 2.5, and usually close to 4. A sersic of n=4 is a classic de Vaucouleurs elliptical galaxy (de Vaucouleurs 1948). The equation for the sersic profile has the form:

$$\Sigma(r) = \Sigma_e \left[-\kappa \left(\left(\frac{r}{r_e} \right)^{\frac{1}{n}} - 1 \right) \right] \tag{2}$$

where Σ is the surface brightness of the galaxy, r_e is the effective radius, within which half of the total light of the galaxy is contained, and Σ_e is the surface brightness at the effective radius.

In Figure 3 everything with a sersic index below 2.5 was classified as a disk and is shown as blue dot and everything with a sersic index above 2.5 as a spheroid, shown with a red dot. As can be seen in Figure 3, it looks as if most of the galaxies selected as quiescent are indeed elliptical like traditional models show, but in the coming section we will show that when they are examined more closely many of them turn out to be disk-like.

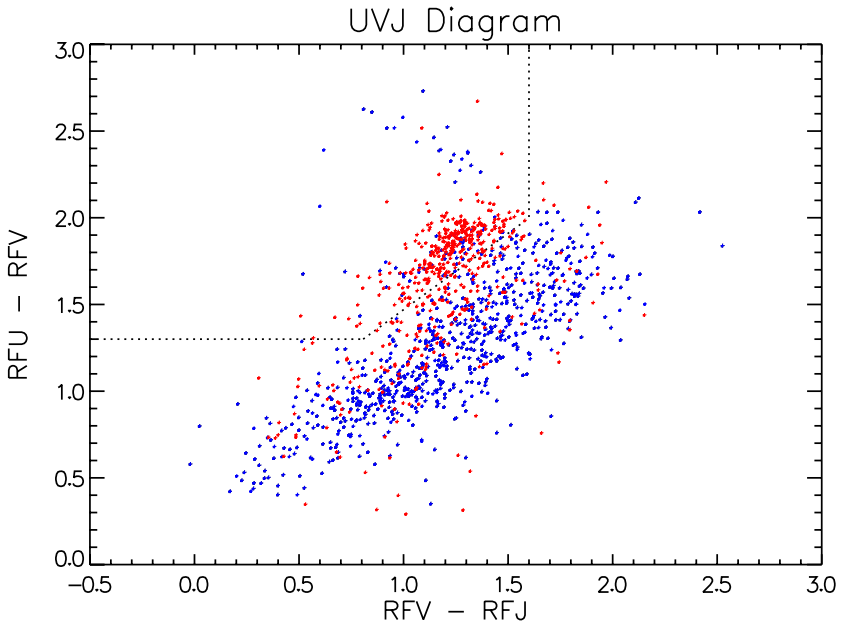

Fig. 3.— UVJ plot of the rest frame visible band minus the J band versus the rest frame ultraviolet band minus the visible band. The blue dots are the galaxies that were classified as disks by a one component galfit (sersic $n < 2.5$) , and the red are the galaxies were classified as elliptical through the same process (sersic $n > 2.5$). The dotted lines separate the quiescent galaxies from the star-forming galaxies and are specified by Williams et al. (2009) and explained in §3.

4. Morphological Classification

After the galaxies were chosen based on the parameters above we were left with a sample size of 140 massive quiescent galaxies over the entire $0.5 < z < 2.5$ redshift range. These 140 galaxies along with information about them are listed in Table 1. In order to determine which of these galaxies were elliptical galaxies and which were disk galaxies we performed both visual classifications of all the galaxies as well as one component and two component fits of them all, using the program GALFIT (Peng et al. 2010).

4.1. Visual Classification

Using the guidelines set by Mark Mozena at the University of California Santa Cruz[1] each galaxy was visually classified as either a spheroid, a disk, something in between, or a completely different irregular shape. A spheroid should be smooth with a concentrated region of light in the center, with possibly a round not quite as dark circle around that, due to the structure of the point spread function (PSF). In Figure 4 the upper left image shows a galaxy that we classified as a spheroid. A disk is characterized by a much more even light distribution (as opposed to the centrally dominated spheroid). Also since disks are flat they will look elongated and not circular if they are seen at any viewing angle besides face-on. The more edge-on they are viewed the more elongated they will appear. We did not see many pure disks in our sample but we saw many bulge dominated disks, meaning that the galaxy contained both a centrally concentrated area of light, but also a disk component. The upper right image in Figure 4 shows a bulge dominated disk. Irregular galaxies are asymmetrical so they do not appear to be either disks or spheroids, and they are usually the product of disturbances or mergers. An irregular galaxy looks like the bottom image in Figure 4. After visually classifying all 140 galaxies, we had an initial number of 34 galaxies that were disk-like.

Along with classifying the main morphology class, we also noted the interaction class of each galaxy. The most highly interacting class is a merger, which are a single object that can have structures such as double nuclei and are usually highly disturbed. Next are galaxies with interacting companions. In order for a galaxy to be classified as interacting there need to be some sort of visible bridge or tidal arm that connects the two galaxies, which can be seen in Figure 4 with the right image in the second row. Continuing on the non-interacting companion comes next. This means that there is another galaxy in the frame of view of

[1]http://www.ucolick.org/∼mmozena/candels_webform/UnifiedWiki_description.pdf

the image, but there is no tidal interaction and the galaxies are not disturbing each other. The galaxy on the left in the second row of Figure 4 has two non interacting companions. Finally many galaxies have no companions at all meaning that they are the only galaxy that appears in the image.

4.2. Galfit Classification

Every galaxy that was visually classified as a disk, bulge dominated disk, or had any disk component, as well as every galaxy that had an original sersic index less than 2.5 was picked out to analyze further with GALFIT. GALFIT is a two dimensional fitting algorithm, which creates a model light profile based on input parameters, a galaxy image, and a point spread function (PSF) (Peng et al. 2010). The program uses four morphology elements (bending, Fourier, coordinate rotation, and truncation modes) in order to be able to recreate features like spiral arms, asymmetries, irregular galaxies and more (Peng et al. 2010), however we used only azimuthally symmetric models to fit our galaxies convolved with the point spread function for our data. Empirical PSFs were derived from stacking the images of several isolated and unsaturated stars in the field. In order to provide a more accurate description of the central region, we replaced the inner-most pixels (within a radius of 3 pixels from the center) with a simulated PSF generated with the TinyTim package (Krist 1995). The TinyTim PSF was dithered and drizzled in the same manner as the observations, and normalized such that the total flux of the newly constructed hybrid PSF model is the same as that of the stacked star. We found this hybrid PSF accurately reproduced the growth curves of stars out to 3". Further details on the PSF models can be found in van der Wel et al. (2012).

For each galaxy we performed both a one component fit, meaning that it would be fit using only a disk or only a spheroid, and a two component fit, which would automatically

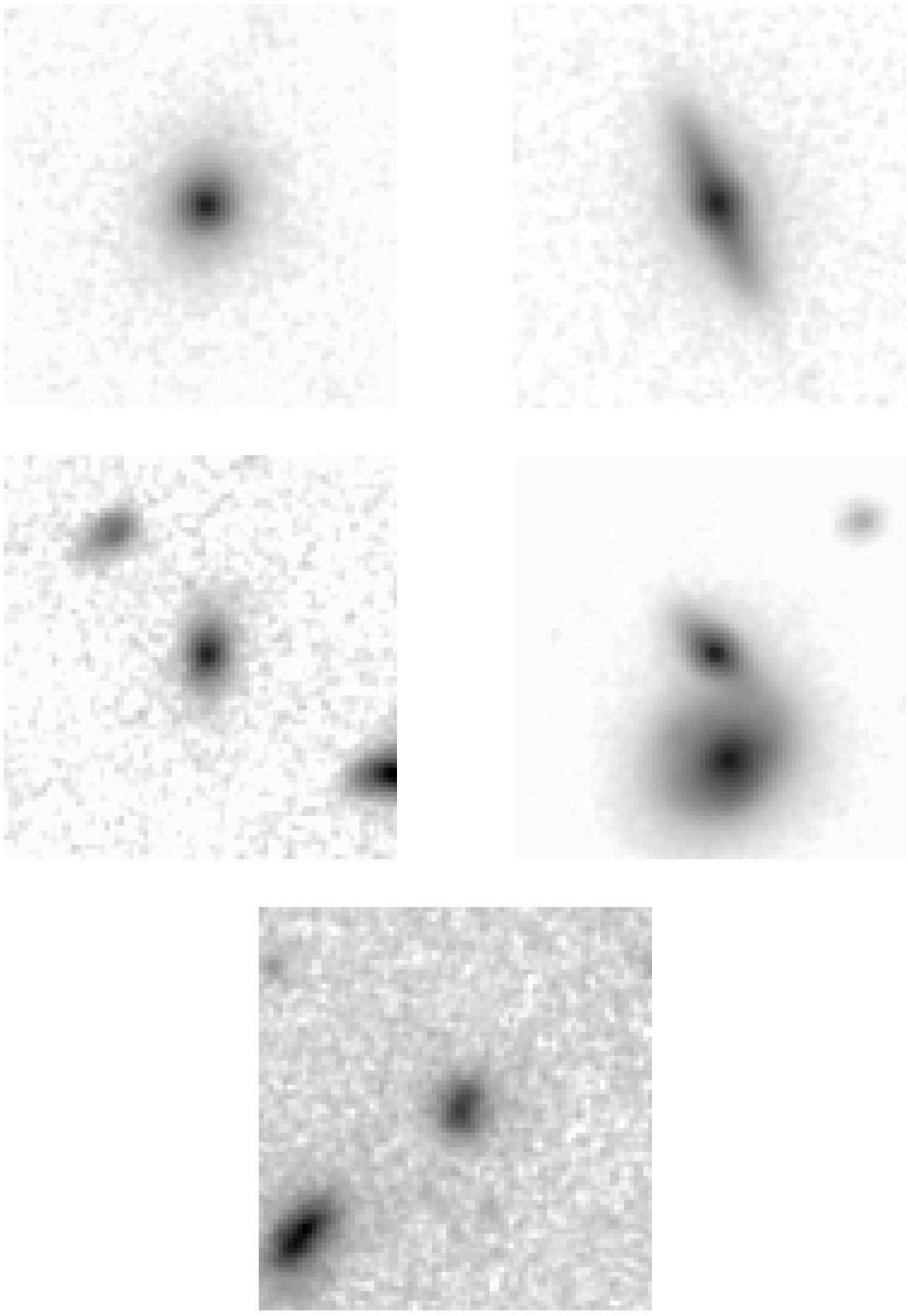

Fig. 4.— images of five different galaxies from our sample of quiescent galaxies all shown in the H-band (1630 nm). Each image is 5" on a side. Going from left to right, up to down, the first galaxy was classified as a spheroid, the second a bulge dominated disk, the third another bulge dominated disk with two companions, the fourth a bulge dominated disk that has an interacting companion, and the last an irregular galaxy with a non interacting companion.

have two structures whether it be a spheroid with a disk or two disks. As for the input parameters, for each galaxy we used 168 × 168 as the size of our convolution box because that was the size of the default PSF, and 12.512 as the magnitude photometric zeropoint. The zeropoint AB magnitude from the WFC3 Data Handbook[2] is 25.96, which we adjusted to our exposure time of 239457.2s, using the following equation:

$$25.96 - 2.5 \times log(EXPTIME) \tag{3}$$

Then separately for all the different galaxies we located the center pixel of the galaxy and measured the size of the image, and we used information from the CANDELS catalog (Guo et al. 2013) to provide an initial estimate for the integrated magnitude, half light radius, sersic index and axis ratio. For the one component models we left the second component blank and allowed the sersic index to vary as it was fitting the galaxy. For the two component models we filled in the the same information for both components except for the sersic indices, the first of which we set to 2.5 and allowed it to vary and the second we set to 1.0 and held it constant. We did this because we wanted to make sure that it was attempting to fit a disk to the galaxy and not just two elliptical shapes. Even though we forced galfit to fit a disk component, it should be noted that if the galaxy is truly bulge-dominated, galfit places most of the light in the component where we allowed the Sersic index to vary freely. Therefore, we expect that bulge-dominated systems will have a greater fraction of their light in a high-sersic component, as opposed to the disk component.

Figure 5 shows three different galaxies and their resulting GALFIT models. First it shows a galaxy that worked well with a one component fit. Next, it shows one that was not fit well with a one component and the same galaxy done with a two component fit,

[2]http://www.stsci.edu/hst/wfc3/documents/handbooks/currentDHB/wfc3_cover.html

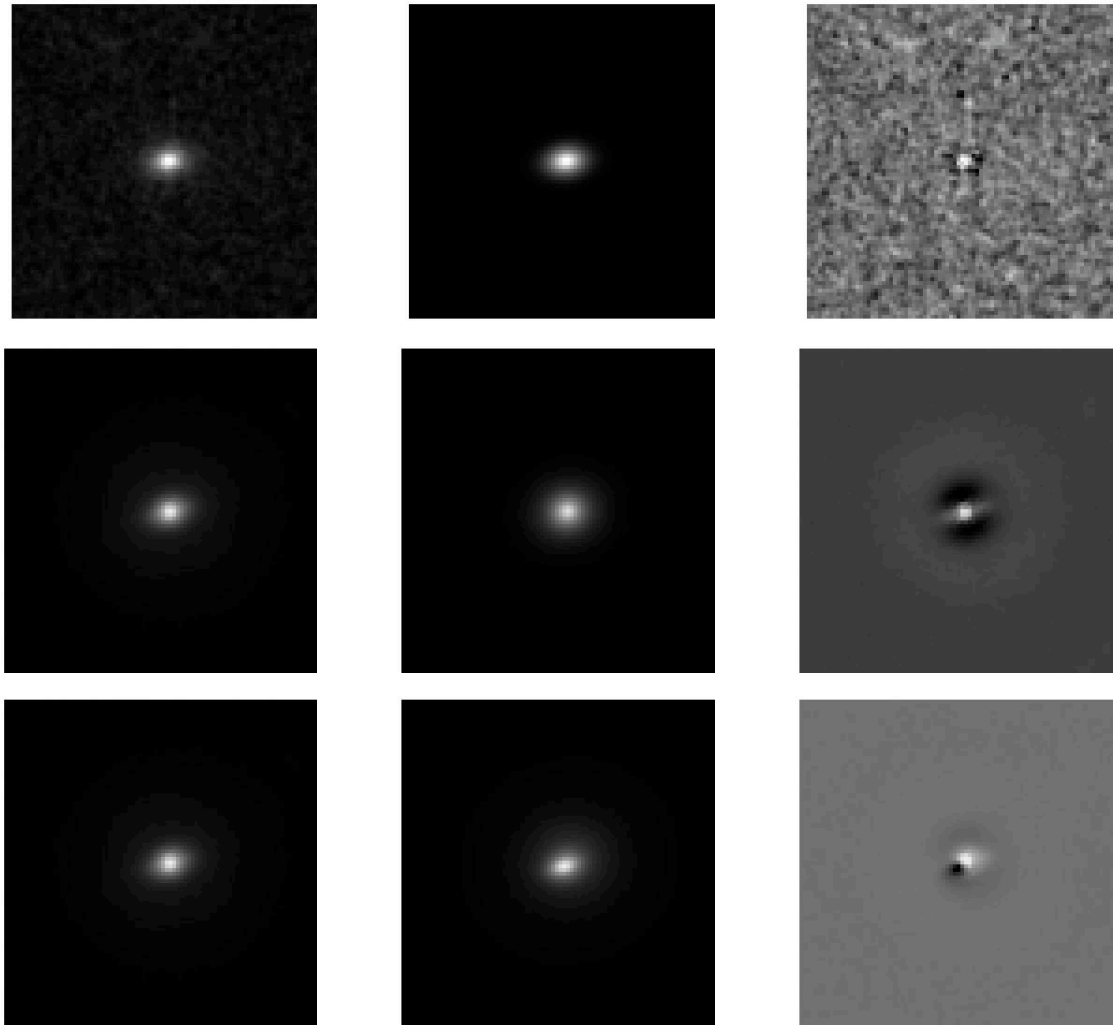

Fig. 5.— GALFIT modeling results, where each row shows a different series. The first image in each row is the original image of the galaxy, the second is the model image that GALFIT produced and the third is the subtracted image of the first two. The first and second rows show one component models and the third row is the same galaxy as the second row, but done with a two component model.

giving much better results. It is easy to tell if a model gives a good fit or not by looking at the subtracted image. A good fit would optimally show a uniform distribution of light pixels, and no obvious galactic structure. The top galaxy has only a slight over-brightness in the center, which is pretty unavoidable, and is basically isotropic besides that. The middle galaxy's subtraction has very obvious structure, including a light colored disk, meaning that the model did not have enough of a disk. That same galaxy, fit with two components has a much better subtraction. Even though it is still not perfect, it only has one over-subtracted area and one under-subtracted spot.

After doing one component and two component fits on all of the 34 galaxies that were selected we found that 23 of them were classified as disk-dominated by GALFIT. In order for the galaxy to be considered disk-dominated it had to either have the one component fit give a sersic index less than 2.5 or have a two component fit with a bulge-to-disk ratio less than 1.0. The bulge to disk ration gives how much light is coming from the bulge component and disk components, so any ratio smaller than 1.0 means that more than half of the light is coming from the disk so the galaxy is disk-dominated. All of our classifications for the 140 galaxies can be seen in Table 2.

5. Results

We split all 140 of the galaxies up into equal redshift bins to see how the percentage of disk galaxies changed over time. Figure 6 shows the results and as expected there are not as many massive disk galaxies in our present universe, but as we go back in time the percentages go up. At our highest redshift bin ($1.58 < z < 2.5$) 29% of the galaxies observed were disk-dominated. The error bars extend up to 42% and the previous studies found around 50% with large errors as well so there is agreement between the two studies. The 29% fraction we find is a significant fraction of the galaxies and therefore we come to the

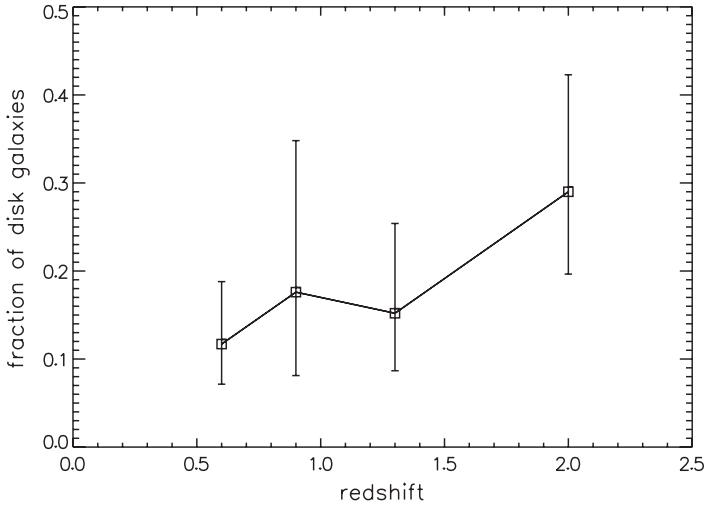

Fig. 6.— The graph shows the percentage of disk galaxies in four equal redshift bins. The first bin was redshift 0.5 to 0.74, then 0.74 to 1.07, 1.07 to 1.58 and finally 1.58 to 2.5. The error bars are are given by Poissonian error limits at a one sigma confidence, which were developed by Ebeling (2003).

conclusion that these massive quiescent disk galaxies do exist and probably in large numbers. It is still unclear exactly what percentage of z $\sim$ 2 galaxies are disk-dominated because even though we examined about ten times more data as earlier studies we still have pretty low number statistics.

In order to gain insight on how these galaxies form we examined some of the properties of the disk galaxies versus the spheroidal galaxies. Since the currently favored model for the formation of massive galaxies is through mergers we did a companion comparison to see if these two types of galaxies live in different environments. Figure 7 shows the results of the companion comparison. Only 24% of the disk-dominated galaxies have a companion in the 5" $\times$ 5" image (approximately 42.5 kpc at the median redshift of the sample), whereas 48% of elliptical galaxies have companions. Even though the 1σ error bars are significant they do not overlap, which gives a hint that these two types of galaxies live in different

environments. The disk galaxies seem to live in more sparsely populated areas, whereas the elliptical galaxies live in much more densely populated areas.

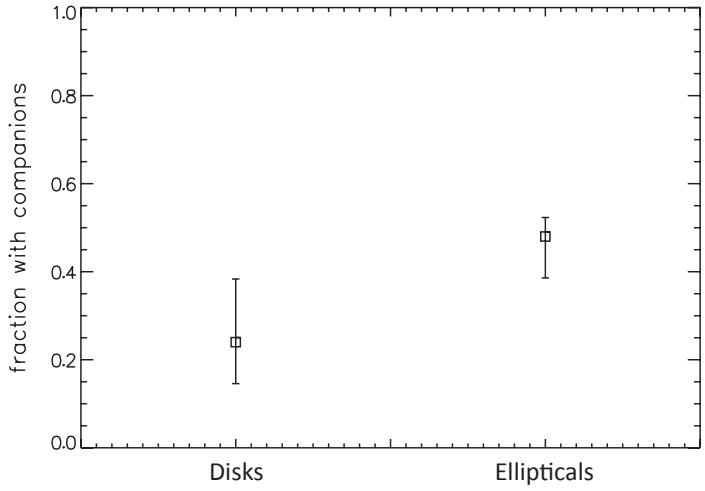

Fig. 7.— Comparison of the companions of the disk-dominated galaxies versus the elliptical galaxies. The fraction refers to the number of disks with a companion divided by the total number of disks. To decide these percentages, any of the 5" × 5" images that had more than one galaxy present was determined to have a companion and we did not discern between interacting and non-interacting companions. Again we used the Poissonian error bars to a one sigma degree of confidence (Ebeling 2003).

6. Discussion and Conclusion

Because we observed a significant fraction of massive quiescent disk galaxies, and these galaxies cannot be created in the traditional merger model there needs to be some other mechanism to form these massive quiescent disks. The companion comparison also suggests that there may be two different methods for forming massive galaxies since the massive elliptical galaxies and the massive disk-dominated galaxies seem to live in two different

environments. Since the massive elliptical galaxies live in more densely populated areas it makes sense that they would form from mergers, but the disk-dominated massive galaxies on average have much fewer companions so maybe mergers are not the answer for their formation. There still is not a dominant theory for their formation because no one knew these galaxies existed until very recently. In the early universe when the massive quiescent galaxies were forming, gas was much more abundant. Simulations of gas rich mergers often show that the end product has a disk component but also a dense core, or a significant bulge component. Most of the galaxies in our sample, even when they were categorized as disk dominant, had spheroidal components at the center. Another way to get this type of galaxy is to have monolithic collapse, which is extremely efficient star formation. In order to create a quiescent disk the gas needs to settle into the disk, but then all the gas has to be completely used up and it has to happen quickly so that the stars are still in a disk but no gas remains for new stars to continue to form. This method does not seem likely because the matter overdensities would have had to be extremely large in order for a massive galaxy to form through gravitational collapse alone. Adding cold streams into this model is a way that was suggested to fix this problem. In the early universe gas and matter were present in much higher densities and not always part of galaxies, so cold accretion of this material along filaments from far away was possible. Cold streams can add enough mass to create galaxies that are the size of those in our sample, and they may result in an extremely efficient star formation rate (Kereš et al. 2005; Dekel & Birnboim 2006).

The next question to address is how did the massive disk galaxies evolve into the massive elliptical galaxies that we see in our local universe. From z $\sim$ 2.5 to the present universe it is expected that these galaxies would undergo some type of merger, whether it be frequent minor mergers or the rare major merger (van der Wel et al. 2011). Both types of mergers can destroy the disk and create an elliptical galaxy since when the disks collide the stars are sent into much more random orbits and are no longer orbiting in the ordered flat disks.

Therefore in the local universe it makes sense that disks no longer exist in massive galaxies because they have been destroyed by merger events that are predicted to happen at some point during their evolution.

In order to confirm these initial results we would really like to extend our analysis to much more data so that our results are more statistically significant. CANDELS has five fields and we only analyzed one of them. We believe that we see some trends forming but our error bars are so large that it is difficult to say exactly what we are seeing. With more galaxies we would be able to say with much more certainty that massive quiescent disk dominated galaxies do exist in abundance and we would be closer to narrowing down a mechanism for their formation if we knew more about their properties and the environments that they live in.

Table 1. Sample of Massive Quiescent Galaxies in GOODS-S.

Galaxy ID[a]	RA[a]	Dec[a]	F160W_mag[a]	Redshift[b]	log(mass)$M_{\odot}$[c]
3145	53.117035	-27.867321	19.43	0.56	10.70
3588	53.086720	-27.862324	20.51	0.62	10.44
3622	53.103654	-27.861062	22.79	1.56	10.53
3527	53.116161	-27.861217	19.41	0.52	10.60
3792	53.089750	-27.859256	19.95	0.54	10.44
3872	53.062415	-27.857515	19.57	0.68	10.83
4162	53.052589	-27.851540	21.07	1.29	11.04
4183	53.062323	-27.851259	22.67	1.67	10.70
4200	53.061901	-27.851046	22.31	1.83	10.86
4240	53.092208	-27.850528	20.74	0.73	10.46
4272	53.096906	-27.850509	20.85	0.96	10.74
4380	53.076400	-27.848664	20.82	1.54	11.11
4379	53.125370	-27.850073	19.83	0.73	10.84
4469	53.061582	-27.847114	20.42	0.51	10.37
4663	53.100047	-27.844172	21.51	1.09	10.55
4794	53.164420	-27.842171	20.26	0.58	10.45
4850	53.125130	-27.840751	22.19	0.99	10.17
4899	53.145923	-27.839971	23.29	1.58	10.33
5039	53.135717	-27.839524	19.17	0.56	10.94
5145	53.126968	-27.837501	20.63	0.52	10.12
5195	53.104996	-27.835936	21.70	1.10	10.53

Table 1—Continued

Galaxy ID[a]	RA[a]	Dec[a]	F160W_mag[a]	Redshift[b]	log(mass)$M_{\odot}$[c]
5205	53.109218	-27.835700	23.00	1.51	10.28
5214	53.184560	-27.836039	21.60	1.04	10.43
5236	53.069555	-27.835720	21.21	0.73	10.37
5267	53.069876	-27.835489	21.52	0.73	10.05
5313	53.127130	-27.834563	21.63	1.68	11.15
5355	53.150191	-27.834531	21.46	1.61	11.01
5383	53.156298	-27.833292	23.31	1.54	10.41
5390	53.209139	-27.833633	22.33	1.30	10.38
5403	53.074411	-27.835288	18.55	0.56	10.96
5522	53.192114	-27.831520	22.34	1.28	10.53
5503	53.168025	-27.832509	21.15	0.66	10.12
5547	53.077159	-27.832744	19.82	0.61	10.64
5610	53.054962	-27.831053	21.18	0.68	10.30
5783	53.129562	-27.827649	22.95	1.51	10.59
5808	53.185227	-27.827835	21.45	1.02	10.41
5849	53.141883	-27.827168	21.83	0.83	10.26
5878	53.188116	-27.827764	20.68	1.12	10.96
5968	53.093900	-27.825721	22.60	1.83	10.49
5986	53.186220	-27.825200	22.74	1.93	10.58
5690	53.054230	-27.829495	19.15	0.60	10.91
5961	53.171696	-27.825660	21.95	1.72	10.97

Table 1—Continued

Galaxy ID[a]	RA[a]	Dec[a]	F160W_mag[a]	Redshift[b]	log(mass)$M_{\odot}$[c]
6028	53.128476	-27.825497	22.18	1.00	10.18
6050	53.161743	-27.824571	21.46	0.82	10.34
6118	53.186134	-27.823398	22.26	1.33	10.54
5631	53.066549	-27.828707	19.48	0.67	10.92
6105	53.097029	-27.823910	21.60	1.16	10.66
6073	53.164746	-27.824550	20.15	0.66	10.55
6399	53.193203	-27.820209	21.02	0.68	10.29
6422	53.100233	-27.819841	20.94	0.58	10.10
6500	53.164995	-27.819335	19.59	0.98	11.26
6739	53.216676	-27.814341	22.99	1.75	10.74
6780	53.132377	-27.814239	21.71	0.74	10.14
6899	53.084273	-27.814037	19.38	0.74	10.98
6921	53.200553	-27.812485	20.54	0.67	10.46
7176	53.083052	-27.808660	20.73	0.67	10.37
7233	53.114834	-27.807065	23.35	2.08	10.61
7266	53.116509	-27.806746	22.35	2.23	11.04
7291	53.047269	-27.806771	21.51	0.68	10.08
7350	53.044729	-27.805384	22.07	1.72	11.03
7495	53.123109	-27.803390	22.12	2.35	11.21
7488	53.084331	-27.805099	19.91	0.73	10.74
7581	53.137766	-27.802094	21.82	1.19	10.59

Table 1—Continued

Galaxy ID[a]	RA[a]	Dec[a]	F160W_mag[a]	Redshift[b]	log(mass)$M_{\odot}$[c]
7610	53.072052	-27.802088	21.06	0.74	10.28
7486	53.047874	-27.804344	18.46	0.55	11.07
7691	53.072668	-27.801498	20.56	0.73	10.58
7838	53.186412	-27.798117	23.38	1.33	10.00
7861	53.108039	-27.797541	23.59	1.82	10.19
7873	53.140306	-27.797526	22.64	1.39	10.49
7843	53.162999	-27.797658	23.11	1.98	10.61
7943	53.075792	-27.796275	22.33	0.91	10.08
7897	53.158804	-27.797156	22.18	1.91	10.93
7962	53.066761	-27.797223	21.27	1.30	10.81
7868	53.163412	-27.799546	19.65	0.68	10.86
8053	53.078291	-27.795720	21.18	0.74	10.30
7876	53.148958	-27.799689	19.36	0.65	10.90
8270	53.078589	-27.792892	21.02	0.73	10.33
8233	53.061818	-27.793981	20.90	0.74	10.35
8388	53.125084	-27.790776	21.19	1.55	11.18
8402	53.068879	-27.790901	20.30	0.73	10.61
8349	53.051936	-27.791442	20.94	1.03	10.68
8490	53.075003	-27.789735	21.22	0.71	10.30
8485	53.045541	-27.789308	20.81	1.22	10.91
8489	53.200372	-27.789844	20.04	0.51	10.52

Table 1—Continued

Galaxy ID[a]	RA[a]	Dec[a]	F160W_mag[a]	Redshift[b]	log(mass)$M_{\odot}$[c]
8527	53.082802	-27.789228	20.53	0.73	10.57
8583	53.080705	-27.787842	22.41	1.12	10.28
8625	53.106597	-27.787300	22.39	2.15	10.91
8686	53.074757	-27.789300	19.19	0.73	11.23
8796	53.202312	-27.785429	22.49	1.68	10.79
8815	53.074023	-27.787464	20.32	0.73	10.66
8871	53.065873	-27.787109	19.54	0.74	10.92
8830	53.135733	-27.784929	23.01	1.34	10.23
8564	53.155447	-27.791492	18.77	0.67	11.14
8968	53.092426	-27.783252	22.77	1.78	10.74
8850	53.165163	-27.785866	21.15	1.32	10.95
9037	53.118487	-27.784351	19.92	0.67	10.70
9060	53.111134	-27.783041	21.10	0.74	10.31
8970	53.121727	-27.785434	19.61	0.67	10.85
9063	53.173678	-27.782063	23.64	1.97	10.45
8814	53.172525	-27.788107	19.56	0.63	10.84
8715	53.075056	-27.788482	18.15	0.73	11.57
9260	53.071643	-27.780322	21.05	0.74	10.33
9378	53.102722	-27.777606	22.94	1.78	10.60
9539	53.046949	-27.775117	23.50	1.57	10.26
9651	53.043833	-27.774705	21.79	1.62	10.99

Table 1—Continued

Galaxy ID[a]	RA[a]	Dec[a]	F160W_mag[a]	Redshift[b]	log(mass)$M_{\odot}$[c]
9654	53.052203	-27.774770	21.25	1.69	11.28
9652	53.080171	-27.775603	19.95	0.74	10.81
9677	53.207680	-27.774077	23.09	2.18	10.58
9730	53.045747	-27.773190	23.15	1.60	10.42
9750	53.060159	-27.773469	20.89	0.74	10.37
9635	53.153813	-27.774572	22.53	1.39	10.50
9785	53.101617	-27.773414	20.93	0.89	10.59
9832	53.046612	-27.772185	22.67	1.60	10.62
9812	53.049977	-27.772486	21.74	1.03	10.37
9797	53.044947	-27.774393	20.58	1.61	11.47
9906	53.075805	-27.771132	23.20	1.66	10.50
9909	53.128520	-27.772700	20.77	1.02	10.67
9930	53.103336	-27.771637	21.31	1.31	11.00
10042	53.071486	-27.769787	22.53	1.33	10.63
10142	53.070069	-27.768059	23.03	1.80	10.70
10193	53.074017	-27.767494	22.82	1.17	10.27
10267	53.113894	-27.767551	21.16	0.67	10.22
10262	53.120593	-27.766837	22.49	1.05	10.23
10330	53.119158	-27.765762	23.24	1.63	10.55
10337	53.141017	-27.766727	21.45	1.90	11.14
10299	53.154969	-27.768908	19.47	1.10	11.48

Table 1—Continued

Galaxy ID[a]	RA[a]	Dec[a]	F160W_mag[a]	Redshift[b]	log(mass)$M_{\odot}$[c]
10521	53.109436	-27.764087	21.32	1.22	10.80
10544	53.076868	-27.765521	19.82	0.74	10.87
10854	53.130087	-27.759084	21.65	1.10	10.60
11297	53.174571	-27.753375	22.19	1.85	10.99
11360	53.124248	-27.753000	21.96	1.22	10.56
11373	53.184068	-27.752622	22.71	1.02	10.12
11532	53.152781	-27.750513	22.34	1.02	10.21
11803	53.159406	-27.748640	20.47	0.67	10.53
11845	53.133505	-27.747704	20.68	0.89	10.73
12526	53.179275	-27.738084	22.55	1.18	10.22
12741	53.166826	-27.738511	20.03	0.52	10.21
12788	53.196706	-27.735808	20.13	0.54	10.55
12822	53.190987	-27.735471	20.40	0.54	10.26
12993	53.168822	-27.733249	20.18	0.55	10.55

[a]From Guo et al. (2013)

[b]From Dahlen et al. (2013)

[c]From Mobasher et al. (2013)

Table 2. Our Classification

Galaxy ID	Single Sersic[d]	Visual Classification	Companions	Bulge/Total	Final Classification
3145	4.44	Elongated Spheroid	No	···	Spheroid
3588	1.09	Point Source	Yes	···	Spheroid
3622	7.45	Spheroid	Yes	···	Spheroid
3527	5.76	Elongated Spheroid	No	···	Spheroid
3792	3.39	Spheroid	No	···	Spheroid
3872	2.69	Bulge and Disk	No	0.25	Disk
4162	1.99	Bulge and Disk	No	0.92	Disk
4183	1.52	Spheroid	Yes	0.49	Disk
4200	6.93	Spheroid	Yes	···	Spheroid
4240	1.81	Bulge and Disk	No	0.96	Disk
4272	3.42	Spheroid	No	···	Spheroid
4380	3.61	Spheroid	Yes	···	Spheroid
4379	6.55	Spheroid	No	···	Spheroid
4469	0.38	Point Source	No	···	Spheroid
4663	3.69	Spheroid	Yes	···	Spheroid
4794	1.62	Bulge and Disk	Yes	0.32	Disk
4850	8.00	Spheroid	Yes	···	Spheroid
4899	1.19	Elongated Spheroid	Yes	0.64	Disk
5039	0.21	Point Source	No	···	Spheroid
5145	4.20	Spheroid	Yes	···	Spheroid

Table 2—Continued

Galaxy ID	Single Sersic[d]	Visual Classification	Companions	Bulge/Total	Final Classification
5195	3.16	Spheroid	No	···	Spheroid
5205	5.50	Spheroid	No	···	Spheroid
5214	3.60	Spheroid	Yes	···	Spheroid
5236	0.25	Point Source	No	···	Spheroid
5267	5.22	Spheroid	Yes	···	Spheroid
5313	1.19	Bulge and Disk	No	0.16	Disk
5355	3.36	Spheroid	No	···	Spheroid
5383	2.89	Spheroid	No	···	Spheroid
5390	6.07	Spheroid	Yes	···	Spheroid
5403	0.20	Point Source	No	···	Spheroid
5547	6.01	Spheroid	No	···	Spheroid
5610	3.70	Spheroid	Yes	···	Spheroid
5783	3.33	Spheroid	No	···	Spheroid
5808	3.59	Spheroid	Yes	···	Spheroid
5849	3.01	Spheroid	Yes	···	Spheroid
5878	3.85	Spheroid	Yes	···	Spheroid
5968	3.04	Merger Spheroid	Yes	···	Spheroid
5986	8.00	Spheroid	Yes	···	Spheroid
5690	7.13	Spheroid	Yes	···	Spheroid
5961	3.54	Spheroid	No	···	Spheroid

Table 2—Continued

Galaxy ID	Single Sersic[d]	Visual Classification	Companions	Bulge/Total	Final Classification
6028	8.00	Spheroid	No	···	Spheroid
6050	1.70	Spheroid	Yes	0.35	Disk
6118	2.52	Spheroid	No	···	Spheroid
5631	3.84	Bulge and Disk	No	0.51	Spheroid
6105	3.20	Spheroid	Yes	···	Spheroid
6073	5.69	Spheroid	No	···	Spheroid
6399	2.24	Bulge and Disk	No	0.99	Disk
6422	2.94	Spheroid	No	···	Spheroid
6500	6.19	Spheroid	No	···	Spheroid
6739	1.18	Spheroid	No	0.27	Disk
6780	3.79	Spheroid	No	···	Spheroid
6899	3.37	Bulge and Disk	Yes	0.58	Spheroid
6921	2.62	Spheroid	No	···	Spheroid
7176	2.65	Spheroid	Yes	···	Spheroid
7233	8.00	Spheroid	No	···	Spheroid
7266	2.85	Spheroid	Yes	···	Spheroid
7291	4.40	Spheroid	No	···	Spheroid
7350	1.39	Spheroid	No	0.45	Disk
7495	3.70	Spheroid	No	···	Spheroid
7488	7.61	Spheroid	Yes	···	Spheroid

Table 2—Continued

Galaxy ID	Single Sersic[d]	Visual Classification	Companions	Bulge/Total	Final Classification
7581	4.48	Spheroid	No	···	Spheroid
7610	3.48	Spheroid	Yes	···	Spheroid
7486	5.19	Spheroid Merger	No	0.96	Spheroid
7691	3.63	Spheroid	Yes	···	Spheroid
7838	6.69	Spheroid	Yes	···	Spheroid
7861	5.35	Spheroid	Yes	···	Spheroid
7873	8.00	Spheroid	No	···	Spheroid
7843	1.36	Spheroid	No	0.29	Disk
7943	0.52	Spheroid	Yes	···	Spheroid
7897	2.24	Spheroid	No	0.48	Disk
7962	6.94	Spheroid	Yes	···	Spheroid
7868	4.40	Spheroid	No	···	Spheroid
8053	3.31	Spheroid	No	···	Spheroid
7876	4.48	Spheroid	No	···	Spheroid
8270	3.18	Spheroid	No	···	Spheroid
8233	6.71	Spheroid	No	···	Spheroid
8388	2.19	Bulge and Disk	No	0.21	Disk
8402	4.58	Spheroid	No	···	Spheroid
8349	3.83	Spheroid	Yes	···	Spheroid
8490	3.22	Spheroid	Yes	···	Spheroid

Table 2—Continued

Galaxy ID	Single Sersic[d]	Visual Classification	Companions	Bulge/Total	Final Classification
8485	17.04	Bulge and Disk	Yes	0.69	Spheroid
8489	0.20	Point Source	No	···	Spheroid
8527	3.01	Bulge and Disk	No	0.50	Spheroid
8583	2.91	Spheroid	Yes	···	Spheroid
8625	5.16	Spheroid	Yes	···	Spheroid
8686	6.00	Spheroid	Yes	···	Spheroid
8796	3.84	Spheroid	No	···	Spheroid
8815	4.03	Spheroid	Yes	···	Spheroid
8871	3.73	Spheroid	No	···	Spheroid
8830	8.00	Spheroid	No	···	Spheroid
8564	4.91	Spheroid	No	···	Spheroid
8968	3.90	Spheroid	No	···	Spheroid
8850	4.00	Spheroid	No	···	Spheroid
9037	5.03	Bulge and Disk	No	0.54	Spheroid
9060	5.51	Spheroid	No	···	Spheroid
8970	5.82	Spheroid	No	···	Spheroid
9063	0.54	Irregular	Yes	0.58	Disk
8814	7.60	Bulge and Disk	No	0.99	Spheroid
8715	4.29	Spheroid	Yes	···	Spheroid
9260	8.00	Spheroid	No	···	Spheroid

Table 2—Continued

Galaxy ID	Single Sersic[d]	Visual Classification	Companions	Bulge/Total	Final Classification
9378	3.20	Spheroid	No	···	Spheroid
9539	1.24	Disk	No	0.23	Disk
9651	3.54	Spheroid	Yes	···	Spheroid
9654	1.68	Bulge and Disk	No	0.28	Disk
9652	5.21	Spheroid	No	···	Spheroid
9677	6.73	Spheroid	Yes	···	Spheroid
9730	6.11	Spheroid	Yes	···	Spheroid
9750	2.95	Spheroid	Yes	···	Spheroid
9635	5.78	Spheroid	No	···	Spheroid
9785	4.05	Spheroid	Yes	···	Spheroid
9832	3.13	Spheroid	No	···	Spheroid
9812	4.55	Spheroid	Yes	···	Spheroid
9797	3.09	Bulge and Disk	Yes	0.93	Spheroid
9906	2.37	Spheroid	No	···	Spheroid
9909	4.50	Bulge and Disk	No	0.55	Spheroid
9930	5.02	Spheroid	No	···	Spheroid
10042	7.05	Spheroid	No	···	Spheroid
10142	8.00	Spheroid	No	···	Spheroid
10193	1.40	Spheroid	Yes	0.46	Disk
10267	20.0	Bulge and Disk	Yes	0.85	Spheroid

Table 2—Continued

Galaxy ID	Single Sersic[d]	Visual Classification	Companions	Bulge/Total	Final Classification
10262	4.10	Spheroid	No	···	Spheroid
10330	2.87	Spheroid	No	···	Spheroid
10337	6.02	Spheroid	Yes	···	Spheroid
10299	5.36	Elongated Spheroid	Yes	0.86	Disk
10521	6.42	Spheroid	No	···	Spheroid
10544	3.04	Bulge and Disk	No	0.48	Disk
10854	4.91	Spheroid	No	···	Spheroid
11297	1.39	Spheroid	No	0.38	Disk
11360	2.89	Spheroid	Yes	···	Spheroid
11373	1.96	Spheroid	Yes	0.71	Disk
11532	3.33	Spheroid	Yes	···	Spheroid
11803	1.94	Bulge and Disk	No	0.31	Disk
11845	1.45	Bulge and Disk	Yes	0.39	Disk
12526	6.26	Spheroid	Yes	···	Spheroid
12741	2.68	Spheroid	No	···	Spheroid
12788	0.28	Point Source	No	···	Spheroid
12822	3.58	Spheroid	Yes	···	Spheroid
12993	0.84	Point Source	No	···	Spheroid

[d]From van der Wel et al. (2012)

REFERENCES

Baldry, I. K., Balogh, M. L., Bower, R., Glazebrook, K., & Nichol, R. C. 2004, The New Cosmology: Conference on Strings and Cosmology, 743, 106

Barnes, J. E. 1988, ApJ, 331, 699

Barnes, J. E., & Hernquist, L. 1992, ARA&A, 30, 705

Bell, E. F., McIntosh, D. H., Katz, N., & Weinberg, M. D. 2003, ApJS, 149, 289

Chang, Y. et al. ApJ, Submitted

Dahlen, et al. ApJ, Submitted

Davis, M., Guhathakurta, P., Konidaris, N. P., et al. 2007, ApJ, 660, L1

Dekel, A., & Birnboim, Y. 2006, MNRAS, 368, 2

de Vaucouleurs, G. 1948, Annales d'Astrophysique, 11, 247

Ebeling, H. 2003, MNRAS, 340, 1269

Fukugita, M., Hogan, C. J., & Peebles, P. J. E. 1998, ApJ, 503, 518

Giavalisco, M., Ferguson, H. C., Koekemoer, A. M., et al. 2004, ApJ, 600, L93

Grogin, N. A., Kocevski, D. D., Faber, S. M., et al. 2011, ApJS, 197, 35

Guo, et al. ApJ, submitted

Hernquist, L. 1992, ApJ, 400, 460

Kereš, D., Katz, N., Weinberg, D. H., & Davé, R. 2005, MNRAS, 363, 2

Koekemoer, A. M., Fruchter, A. S., Hook, R. N., & Hack, W. 2002, in The 2002 HST Calibration Workshop, ed. S. Arribas, A. Koekemoer, & B. Whitmore (Baltimore, MD: STScI), 337

Koekemoer, A. M., Faber, S. M., Ferguson, H. C., et al. 2011, ApJS, 197, 36

Labbé, I., Huang, J., Franx, M., et al. 2005, ApJ, 624, L81

Lawrence, A., Warren, S. J., Almaini, O., et al. 2007, MNRAS, 379, 1599

McGrath, E. J., Stockton, A., Canalizo, G., Iye, M., & Maihara, T. 2008, ApJ, 682, 303

Mobasher, et al. ApJ, Submitted

Peng, C. Y., Ho, L. C., Impey, C. D., & Rix, H.-W. 2010, AJ, 139, 2097

Scoville, N., Abraham, R. G., Aussel, H., et al. 2007, ApJS, 172, 38

Toomre, A. 1977, Evolution of Galaxies and Stellar Populations, 401

van der Wel, A., Rix, H.-W., Wuyts, S., et al. 2011, Galaxy Formation,

van der Wel, A., Bell, E. F., Häussler, B., et al. 2012, ApJS, 203, 24

Williams, R. J., Quadri, R. F., Franx, M., van Dokkum, P., & Labbé, I. 2009, ApJ, 691, 1879

Williams, R. J., Quadri, R. F., Franx, M., et al. 2010, ApJ, 713, 738

Windhorst, R. A., Cohen, S. H., Hathi, N. P., et al. 2011, ApJS, 193, 27

Wuyts, S., Labbé, I., Franx, M., et al. 2007, ApJ, 655, 51

This manuscript was prepared with the AAS LaTeX macros v5.2.